Laser and Particle Beams (2000), *18*, 175–181. Printed in the USA.

3D Numerical simulation of Rayleigh–Taylor instability using MAH-3 code

N.N. ANUCHINA, V.I. VOLKOV, V.A. GORDEYCHUK, N.S. ES'KOV, O.S. IIYUTINA, AND O.M. KOZYREV

Russian Federal Nuclear Center, All-Russian Scientific Research Institute of Technical Physics, P.O. 245, Snezhinsk Chelyabinsk Region, Russia 456770

(Received 23 June 1999; Accepted 23 June 1999)

Abstract

A 3D numerical study of the turbulent phase of the evolution of Rayleigh–Taylor instability (RTI) was undertaken using the MAH-3 code. A criterion and a technique have been developed that can be used for diagnostics in computational experiments studying flow transition to self-similar turbulence. It has been found that a criterion of the flow transition to the self-similar turbulence is Kolmogorov's self-similar distribution of the turbulent kinetic energy together with the square law of mixing zone extension. The technique is based on the analysis of the evolution of the dimensionless power spectrum of specific kinetic energy. Three phases of nonlinear mixing are found: "relict chaos", "formation of classical energy spectrum" and "spectrum degradation." Determination of a proportionality factor for a square law within the time range incorporating inertial interval gives the value of $\alpha \approx 0.07$.

1. INTRODUCTION

An interface between two fluids of different densities is unstable and behaves as a RTI if it is affected by acceleration directed from a light fluid to a heavy one. This is true when fluid with the density ρ_2 is above fluid with the density $\rho_1 < \rho_2$ in a gravitational field with acceleration $\vec{g}$. A square law was proposed in Anuchina *et al.* (1978) to describe extension of a turbulent mixing zone after achieving a self-similar phase in the form $L = f(\rho_2/\rho_1)\cdot t^2$. Numerous experimental and numerical studies of turbulent mixing (Anuchina & Ogibina, 1982; Kucherenko *et al.*, 1988; Read, 1984; Youngs, 1984, 1989, 1991, 1992) are devoted to the square law verification and assessment of $f(\rho_2/\rho_1)$.

Yu.A. Kucherenko, K.I. Read, and D.L. Youngs conducted experiments for the substances with various density differences and the experiments showed that the depth of "bubble" penetration could be described with the dependence $L_b = \alpha\cdot A\cdot g\cdot t^2$, where A is an Atwood number and the constant $\alpha \approx 0.06$. Usually a sufficient condition for treating a flow as self-similar turbulent is the realization of the square law for mixing zone extension and spatial-temporal similarity of the averaged density profiles within some time interval. However, to qualify turbulent mixing as self-similar it is necessary to consider the internal features of the flow based on spectral presentation of hydrodynamic fields. This means that in addition to determining spatial-temporal similarity of flow functionals it is necessary to verify whether there exists an inertial interval of wave numbers k within which the Kolmogorov–Obukhov law (Obukhov, 1941*a*, 1941*b*; Kolmogorov, 1941) of turbulent kinetic energy distribution $E(k) \approx k^{-5/3}$ is valid.

Turbulence energy spectrum distribution was used in, for instance, Dalziel *et al.* (1997); Sin'kova *et al.* (1997); Anuchina *et al.* (1997) to analyze the results of numerical simulation of gravity turbulent mixing.

A criterion of determining self-similar turbulent phase of flow can be stated:

- presence of self-similar inertial mechanism of transferring energy of velocity field pulsation at the intermediate range of wave numbers;
- spatial-temporal similarity of a representative enough set of flow functionals.

2. NUMERICAL METHOD AND ITS CAPABILITIES

MAH-3 code is intended to calculate nonstationary 3D hydrodynamic flows of multicomponent media with strongly distorted interface. The code exploits a numerical method based on papers Hirt *et al.* (1974); Pracht (1975); Anuchina *et al.* (1992).

Address correspondence and reprint requests to: O.M. Kozyrev, RFNC-VNIITF, P.O. 245 Snezhinsk, Chelyabinsk Region, Russia 456770. E-mail: o.m.kozyrev@vniitf.ru

The method is based on splitting calculations into Lagrangian and Eulerian phases. Numerical integration zone is considered as a set of physical or computational regions. Each region is a topological parallelepiped. Region boundaries may be either interface surfaces including the selected Lagrangian surfaces or outer problem boundaries: free boundaries, rigid walls, continuous Eulerian boundaries or boundaries with specified pressure.

Two methods are used to describe the interfaces:

- *Regular*: when the interface is described as a coordinate surface of the mesh;
- *Irregular*: when the interface is described with an unstructured mesh of markers and mixed cells.

2.1. Regular method

A mesh cell is a trilinear imaging of a cube on 3D physical space when the cell vertexes are the images of cube vertexes. Different equations for each phase are derived through approximation of conservation laws formulated for a control volume, that is, the scheme is divergent with respect to mass, momentum and total energy. Integration is performed in two stages. Lagrangian equations are solved at the first stage. The second stage includes convectional flows between the cells if the specified law of mesh movement is not a Lagrangian one. Lagrangian stage calculations can be done using either explicit or implicit schemes. Algorithm of solving implicit difference equations is an iterative Newton–Jacobi process. Values obtained from the explicit scheme are used as initial approximation. The process converges at any time step.

An explicit scheme is used to approximate the convectional flows at the Eulerian stage. Two options are implemented:

- first-order-accuracy approximation using "up-wind" differences (Scheme 1);
- Lax–Wendroff second-order-accuracy approximation (Scheme 2).

Each computational or physical region uses its own hexahedral mesh, which is arbitrary but coordinated at the Lagrangian interface surfaces.

2.2. Irregular method of calculating the contact surfaces

Based on a multi-component one-velocity model, strongly distorted interface between substances has been described. Transition to describing the interface surface with the mixed cells occurs when strong distortions appear and it is no longer possible to calculate the contact surface as a coordinate mesh surface. In this case the contact surface does not coincide with coordinate surface and can intersect arbitrarily Eulerian mesh forming the mixed cells, which contain several different substances. These cells introduce nonregularity in the numerical algorithm at both Lagrangian and Eulerian stages. Conditions of thermodynamic equilibrium of the components and continuity of the velocity vector at the interface are used to calculate the mixture.

Peculiarity of mixed cell calculations at the Lagrangian stage consists in determination of mixture pressure, which in the general case is iterative. Otherwise these cells are calculated as homogeneous ones. Nonregularity at the Eulerian stage considerably complicates the algorithm of calculation of convectional flows. In the vicinity of the mixed cells, convectional flows are calculated with due account of direction of medium flow and composition of substances in the cells. To study interface evolution thoroughly, an unstructured mesh of markers can be used which consists of triangles and is not associated with the integration zone mesh. The appropriate mesh of markers for the interface is maintained by controlling density of the markers, adding new markers and remapping, if necessary. Since the irregular method is time-consuming, the code embeds the option of rebuilding the mesh and calculating the flows once per several Lagrangian steps rather than at each step. Based on *a priori* information about the processes in the specific problem, it is possible to combine Lagrangian (explicit and implicit) and Eulerian calculations, and apply regular or irregular method of describing contact surfaces at different periods of time. This approach allows us to select an optimal way of obtaining the required accuracy.

3. PROBLEM SETUP

In the 3D area (x, y, z) bounded on six sides with rigid walls there are two layers of nonviscous, incompressible and non-heat-conducting substances of different density affected by gravitational field. Gravitational acceleration $\vec{g}$ acts in the negative direction of axis z, from a heavy substance to a light one. Initial conditions are as follows: $L = L_x = L_y = L_z = 15$ cm are the system dimensions, $z_0 = 0.5L_z$ is an initial position of the interface, $g = -0.03435\ \mathrm{cm/mc^2}$, $\rho_1 = 1.0\ \mathrm{g/cm^3}$, $\rho_2 = 2.9\ \mathrm{g/cm^3}$ are densities of the lower and upper layers, respectively. The initial data presented were taken from Youngs (1992).

Fluid incompressibility was simulated by setting an isothermal equation of state $p = c^2 \cdot \rho$ with rather large values of $c^2, c_1^2 = 10^2, c_2^2 = c_1^2(\rho_1/\rho_2)$. At the initial moment of time, density and pressure distribution corresponds to hydrostatic equilibrium. A small-scale random perturbation of the interface with the amplitude $a_0 = 0.01$ was introduced. The initial perturbation contained the whole range of harmonics specified by the difference mesh resolution. The runs considered are follows:

Cc1: $\Delta x = \Delta y = \Delta z = 0.25$, Scheme 1;

Cc2: $\Delta x = \Delta y = \Delta z = 0.25$, Scheme 2;

Bb2: $\Delta x = \Delta y = \Delta z = 0.125$, Scheme 2.

https://doi.org/10.1017/S0263034600182047 Published online by Cambridge University Press

4. PROCESSING OF THE RESULTS

4.1. Width of the turbulent mixing zone

To compare the calculated data with the square law, depth of light-to-heavy penetration L_b is determined as a function of $S = A \cdot g \cdot t^2$. An upper boundary of the mixing zone is defined as a value for which the volume concentration of the light substance averaged over directions x, y equals 5%.

4.2. Spectral properties of the velocity field

Spectral properties of the velocity field are obtained under the following assumptions: Assume, that $\vec{u} = (u, v, w)$ is a velocity vector with the components u, v, w along x, y, and z axes, respectively. In this setup it is valid to treat u as odd periodic in direction x and even periodic in directions y, z; as odd periodic in direction y and even periodic in directions x, z; and w, as odd periodic in direction z, and even periodic in directions x, y with a period of $2L$. Then valid is exact spectral expansion of discrete velocity field:

$$u_{ijk} = \sum_{p=0}^{N_3} \sum_{n=0}^{N_2} \sum_{m=0}^{N_1} \tilde{u}_{mnp} \sin \frac{\pi m}{L} x_{ijk} \cos \frac{\pi n}{L} y_{ijk} \cos \frac{\pi p}{L} z_{ijk},$$

$$v_{ijk} = \sum_{p=0}^{N_3} \sum_{n=0}^{N_2} \sum_{m=0}^{N_1} \tilde{v}_{mnp} \cos \frac{\pi m}{L} x_{ijk} \sin \frac{\pi n}{L} y_{ijk} \cos \frac{\pi p}{L} z_{ijk},$$

$$w_{ijk} = \sum_{p=0}^{N_3} \sum_{n=0}^{N_2} \sum_{m=0}^{N_1} \tilde{w}_{mnp} \cos \frac{\pi m}{L} x_{ijk} \cos \frac{\pi n}{L} y_{ijk} \sin \frac{\pi p}{L} z_{ijk},$$

$$i = 0, \ldots, N_1; \quad j = 0, \ldots, N_2; \quad k = 0, \ldots, N_3. \tag{1}$$

Here, N_1, N_2, N_3 are numbers of mesh nodes in directions x, y, and z, respectively, (i, j, k) is index of a node.

The above representation leads to obvious extension of the discrete velocity field $\vec{u}_{ijk}$ to a continuous $\vec{u}(x, y, z)$ one, and for this purpose it is sufficient to consider $x_{ijk}, y_{ijk}, z_{ijk}$ as continuous arguments. Therefore, when building spectral functionals, the velocity field is considered to be a function of continuous arguments.

4.2.1 Velocity field correlation averaged over sphere and Taylor micro-scale

$$B_{\vec{u}}(\xi, \eta, \zeta) = \frac{1}{8L^3} \int_{-\ell}^{\ell} \int_{-\ell}^{\ell} \int_{-\ell}^{\ell} \vec{u}(x, y, z) \cdot \vec{u}(x + \xi, y + \eta, z + \zeta)\, dx\, dy\, dz$$—velocity field correlation,

$$b_{\vec{u}}(r) = \frac{1}{4\pi} \int_0^{\pi} \int_0^{2\pi} B_{\vec{u}}(r \sin\psi \cos\varphi, r \sin\psi \sin\varphi, r \cos\psi) \times \sin\psi\, d\varphi\, d\psi$$—velocity field correlation averaged over sphere,

$$\beta = \frac{b_{\vec{u}}(r)}{b_{\vec{u}}(0)}$$—averaged over sphere correlation function of the velocity field.

ℓ = Taylor scale equal to the length of a segment cut on the abscissa axis by a parabola which has a second-order tangency with the correlation function graph in its top.

4.2.2 Power spectrum of turbulent specific kinetic energy

$q = \sqrt{(\pi m/L)^2 + (\pi n/L)^2 + (\pi p/L)^2}$ is wave vector modulus, $m = 0, \ldots, N_1$; $n = 0, \ldots, N_2$; $p = 0, \ldots, N_3$; $m^2 + n^2 + p^2 \neq 0$. $q_{\max} = \sqrt{(\pi N_1/L)^2 + (\pi N_2/L)^2 + (\pi N_3/L)^2}$ is a maximal value of the wave vector modulus. The region $(0, q_{\max})$ is uniformly split into N intervals, q_1 is a center of the 1th interval, $1 = 1, \ldots, N$, Δq is the length of the interval. The introduced mesh is used for building turbulent specific kinetic energy power spectrum.

$\tilde{E}(q_1)$ is a partial sum divided by Δq of the series terms for $E = 0.5 b_{\vec{u}}(0)$, terms corresponding to the wave vectors falling into the 1th interval by modulus. Transition to dimen-

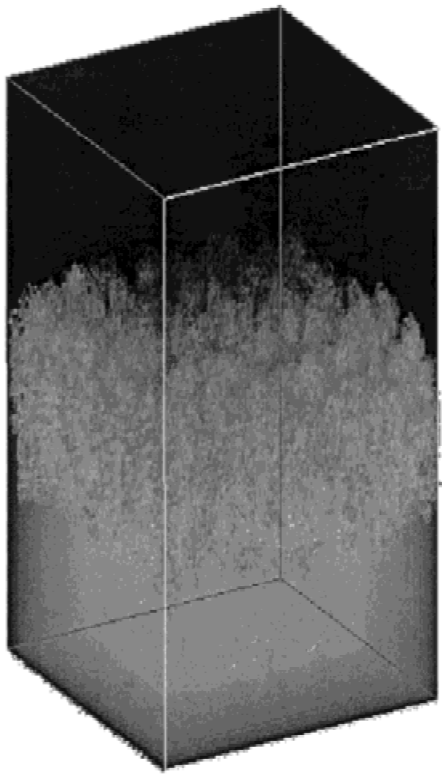

Fig. 1. A typical 3D raster pattern of the density field obtained by 3D numerical simulation of the evolution of Rayleigh–Taylor instability.

https://doi.org/10.1017/S0263034600182047 Published online by Cambridge University Press

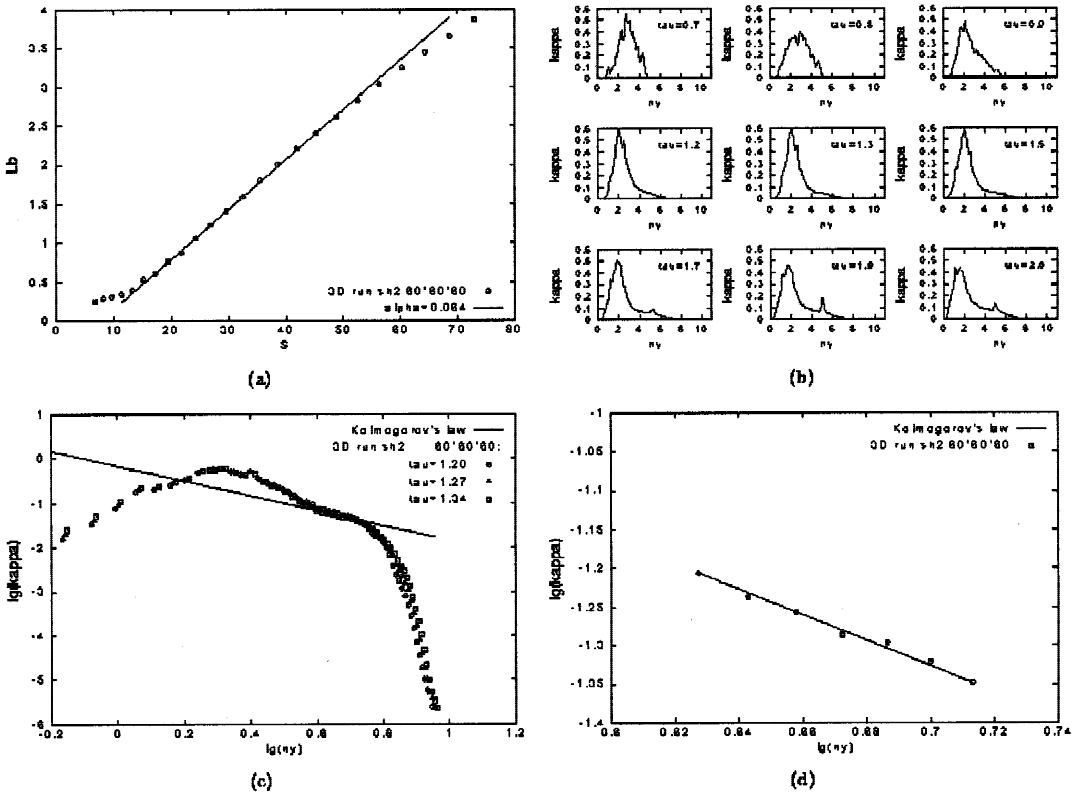

Fig. 2. Results of the Cc2 run with second-order accuracy for 60^3 mesh. (a) Bubble penetration *Lb* (cm) *versus* $S = Agt^2$ (cm). The solid line is the best fit straight line to the mesh data. (b) Dynamics of the turbulent energy power spectrum. Each frame shows dimensionless turbulent energy power spectrum *kappa versus* dimensionless frequency *ny*, where *tau* is dimensionless time. (c) Turbulent energy power spectrum compared to the "five third" law in logarithmic scale. The solid line with the slope $-5/3$ is Kolmogorov's distribution of turbulent kinetic energy. *kappa*, *ny* and *tau* are the same as in (b). (d) "Inertial interval" of turbulent energy power spectrum obtained by averaging over three time moments *tau* = 1.20, 1.27, 1.34 and presented in logarithmic scale. The solid line is the same line as plotted in (c). *kappa* and *ny* are the same as in (b).

sionless dependencies is performed according to the formulas below:

$\kappa(\nu_1) = \tilde{E}(q_1)/\ell E$ is dimensionless power spectrum of turbulent specific kinetic energy, $\nu_1 = \ell \cdot q_1$ is dimensionless frequency, where ℓ is the Taylor scale.

5. RESULTS OF CALCULATIONS

Typical 3D view of the density field obtained by 3D numerical simulation of the evolution of RTI is given in Figure 1. Figure 2 presents the results of run Cc2 processing. Figure 2a gives a plot of light-to-heavy penetration depth *versus S*. It is easy to notice that the slope α of the curve varies. Therefore, it is necessary to select a time interval to be used for determining α. This should be the time interval, which best fits the today's understanding of self-similar turbulence. For this purpose, analyze the power spectrum of turbulent specific kinetic energy.

According to A. Kolmogorov's hypothesis, in self-similar turbulence case the wave number scale consists of three characteristic intervals: energy interval where major fraction of pulsation energy is concentrated; inertial interval where energy is transferred to the large wave numbers of the spectrum; and dissipation interval where most of turbulent energy is dissipated. If energy and dissipation intervals do not overlap considerably, inertial interval must be between the frequencies corresponding to the maximal energy and dissipation (Monin & Yaglom, 1967).

Nine frames in Figure 2b illustrate dynamics of turbulent specific kinetic energy power spectrum as a function of dimensionless time $\tau = t \cdot \sqrt{Ag/L}$. In terms of spectrum, the flow development can be described as follows:

- *Relict chaos*: Inertia and dissipation have not yet finished selection of perturbations from the initial spectrum with respect to frequency, energy is transferred in spectrum in both directions: from large to small frequencies and from small to large frequencies;
- formation of *Classical energy spectrum*: spectrum plot becomes of typical asymmetrical "cap"-like shape;
- *Spectrum degradation*: energy spectrum changes qualitatively and quantitatively. In this case, changes occur due to additional scale in short-wave spectrum.

https://doi.org/10.1017/S0263034600182047 Published online by Cambridge University Press

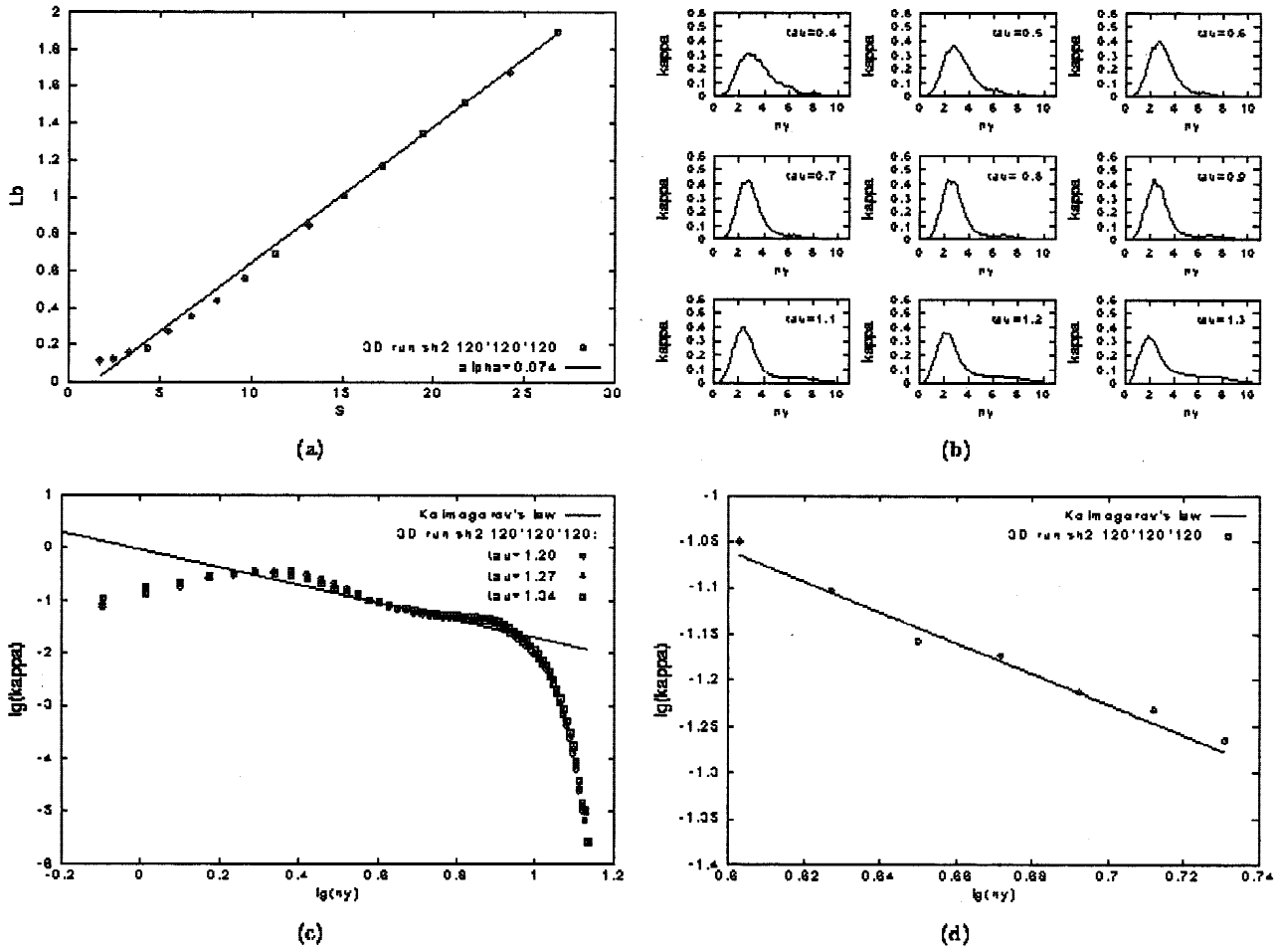

Fig. 3. Results of the Bb2 run with second-order accuracy for 120^3 mesh. (a) Bubble penetration *Lb* (cm) *versus* $S = Agt^2$ (cm). The solid line is the best fit straight line to the mesh data. (b) Dynamics of the turbulent energy power spectrum. Each frame shows dimensionless turbulent energy power spectrum *kappa versus* dimensionless frequency *ny*, where *tau* is dimensionless time. (c) Turbulent energy power spectrum compared to the "five-third" law in logarithmic scale. The solid line with the slope $-5/3$ is Kolmogorov's distribution of turbulent kinetic energy. *kappa*, *ny* and *tau* are the same as in (b). (d) "Inertial interval" of turbulent energy power spectrum obtained by averaging over three time moments *tau* = 1.20, 1.27, 1.34 and presented in logarithmic scale. The solid line is the same line as plotted in (c). *kappa* and *ny* are the same as in (b).

It can be stated that frames with $\tau = 0.7$–0.9 correspond to the first phase; with $\tau = 1.2$–1.5—to the second and with $\tau = 1.7$–2.0—to the third. Boundaries between three above phases are rather conventional, but qualitatively correct. The slope of the curve L_b *versus* S was determined from five calculated second-phase points corresponding to $\tau = 1.1$–1.3. In Figure 2a, a line with the obtained slope $\alpha = 0.064$ is shown. It is obvious from the figure that the slope would be less if calculated from the third-phase points. Figure 2c presents in logarithmic scale the spectra of turbulent specific kinetic energy for $\tau = 1.20, 1.27, 1.34$ in comparison with the line corresponding to the "five-thirds" law. On the whole it can be stated that self-similarity takes place within "inertial interval". Profiles at this interval coincide better than at other intervals. The slope determined at the "inertial interval" from the spectrum averaged over three time moments is equal to -1.59 that differs by 5% from the theoretical value of $-5/3$ (Fig. 2d).

Figure 3b illustrates dynamics of turbulent specific kinetic energy power spectrum in the run Bb2 for $\tau = 0.4$–1.3. Unlike run Cc2, formation of "classical energy spectrum" starts earlier and has both a longer duration and more stationary profiles. Time moments $\tau = 1.1$–1.3 can be referred to it. Figure 3a shows depth L_b of light-to-heavy penetration *versus* S. Slope $\alpha = 0.074$ is calculated from five points corresponding to $\tau = 1.1$–1.3. A line with this slope is plotted in Figure 3a. In Figure 3c spectra of turbulent specific kinetic energy are plotted for $\tau = 1.20, 1.27, 1.34$ in comparison to the "five thirds" law. It can be stated, in this run the "inertial interval" is displayed more and Kolmogorov's self-similarity factor determined within the "inertial interval" from the spectrum averaged over three time moments is equal to -1.62 that coincides with the theoretical value to the accuracy of 3% (Fig. 3d).

The run Cc1 is performed under first-order-accuracy scheme, the number of points in each direction being two

https://doi.org/10.1017/S0263034600182047 Published online by Cambridge University Press

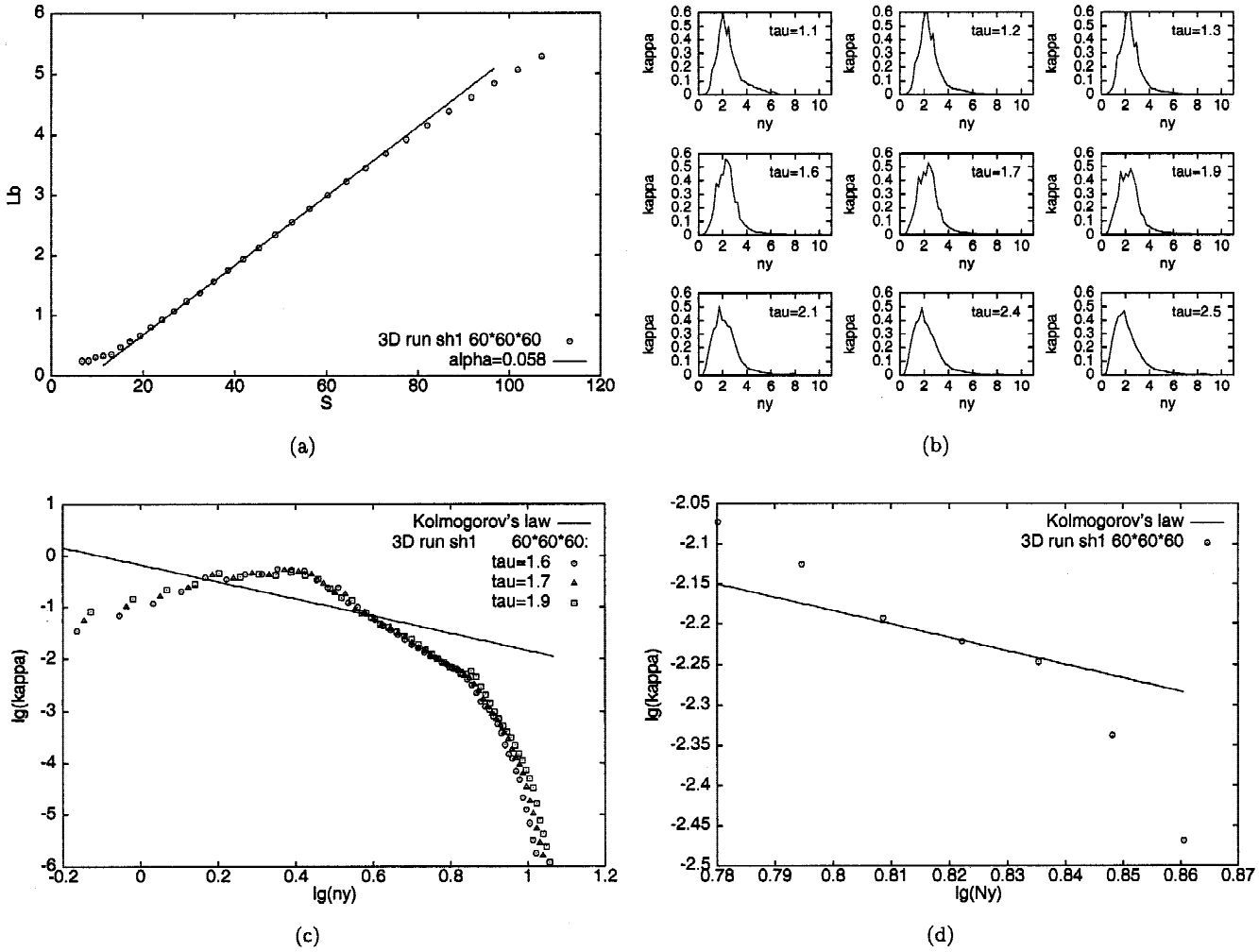

Fig. 4. Results of the Cc1 run with first-order accuracy for 60^3 mesh. (a) Bubble penetration *Lb* (cm) *versus* $S = Agt^2$ (cm). The solid line is the best fit straight line to the mesh data. (b) Dynamics of the turbulent energy power spectrum. Each frame shows dimensionless turbulent energy power spectrum *kappa versus* dimensionless frequency *ny*, where *tau* is dimensionless time. (c) Turbulent energy power spectrum compared to the "five third" law in logarithmic scale. The solid line with the slope $-5/3$ is Kolmogorov's distribution of turbulent kinetic energy. *kappa*, *ny* and *tau* are the same as in (b). (d) "Inertial interval" of turbulent energy power spectrum obtained by averaging over three time moments *tau* = 1.6, 1.7, 1.9 and presented in logarithmic scale. The solid line is the same line as plotted in (c). *kappa* and *ny* are the same as in (b).

times less than in the run Bb2. Hence, due to larger overlapping of the energy and dissipation intervals than in the runs Cc2 and Bb2, "classical energy spectrum" phase is practically absent. This is demonstrated in Figure 4 where spectra of specific turbulent energy are plotted and for $\tau = 1.6$, 1.7, and 1.9 spectra are compared in log scale to "five-thirds" law. The presented spectra are degraded, delta-like plots are typical of them, and almost all energy is concentrated within a small frequency range corresponding to hydrodynamic scale. Factor $\alpha = 0.058$ was obtained from five points corresponding to $\tau = 1.6$–1.9.

6. CONCLUSIONS

1. Analysis of dynamics of turbulent specific kinetic energy power spectrum has shown that there are three phases of turbulent mixing: "relict chaos", "classical energy spectrum", and "spectrum degradation".
2. In calculations energy and dissipation ranges can overlap significantly due to a small number of points and excessive dissipation of the difference scheme. This leads to an absent phase of formation and existence of the classical spectrum of turbulent kinetic energy. Without energy spectrum control, determination of slope α might give information irrelevant to self-similar turbulence.
3. Slope calculation within the time interval corresponding at some extent to existence of inertial interval has given the value of $\alpha \approx 0.07$, smaller values of α correspond to the phase of degraded spectrum when extension of the mixing zone depends mostly on large-scale perturbations of energy spectrum.

https://doi.org/10.1017/S0263034600182047 Published online by Cambridge University Press

ACKNOWLEDGMENT

The work was performed under ISTC Project #177.

REFERENCES

ANUCHINA, N.N. *et al.* (1978). Turbulent Mixing at the Accelerating Interface between Fluids with Different Densities. *News of the USSR Academy of Science, Ser.: Fluid and Gas Mechanics*, **6**, 157.

ANUCHINA, N.N. & OGIBINA, V.N. (1982). Numerical Simulation of Gravitational Turbulent Mixing. *VANT*, **2**, 10.

ANUCHINA, N.N. *et al.* (1992). Report at Russian/U.S. Weapons Laboratories introductory technical exchange in computation and computer science. Lawrence National Laboratory, Livermore, California.

ANUCHINA, N.N. *et al.* (1997). Proceedings of the sixth international workshop on the physics of compressible turbulent mixing, (Jourdan, G., & Houas, L., Eds.) Marseille, France.

DALZIEL, S.B. *et al.* (1997). Proceedings of the sixth international workshop on the physics of compressible turbulent mixing, (Jourdan, G., & Houas, L., Eds.) Marseille, France.

HIRT, C.W. *et al.* (1974). An arbitrary Lagrangian–Eulerian computing method for all flow speed. *J. of Comput. Physics* **14**, 3.

KOLMOGOROV, A.N. (1941). Local Structure of Turbulence in Incompressible Fluid at Very Large Reynolds Numbers. *Reports of the USSR Academy of Science*, **30**, 4.

KUCHERENKO, YU.A. *et al.* (1988). Experimental Study of Gravitational Turbulent Mixing in Self-Similar Mode. *VANT*, **1**, 1.

MONIN, A.S. & YAGLOM, A.M. (1967). Statistical Hydromechanics, Part 2 ("Nauka", Moscow).

OBUKHOV, A.M. (1941*a*). On Energy Distribution In Turbulent Flow Spectrum. *Reports of the USSR Academy of Science*, **32**, 1.

OBUKHOV, A.M. (1941*b*). On Energy Distribution In Turbulent Flow Spectrum. *News of the USSR Academy of Science, Ser.: Geography and Geology*, **5**, 5.

PRACHT, W.E. (1975). Calculating three-dimensional fluid flows at all speeds with an Eulerian–Lagrangian computing mesh. *J. of Comput. Physics*, **17**, 3.

READ, K.I. (1984). Experimental investigation of turbulent mixing by Rayleigh–Taylor instability. *Physica* **12D**, 45.

SIN'KOVA, O.G. *et al.* (1997). Three-dimensional numerical simulation of gravitational turbulent mixing. *Proceedings of the sixth international workshop on the physics of compressible turbulent mixing* (Jourdan, G., & Houas, L., Eds.). Marseille, France.

YOUNGS, D.L. (1984). Numerical simulation of turbulent mixing by Rayleigh–Taylor instability. *Physica* **12D**, 32.

YOUNGS, D.L. (1989). Modeling turbulent mixing by Rayleigh–Taylor instability. *Physica* **37D**, 270.

YOUNGS, D.L. (1991). Three dimensional numerical simulation of turbulent mixing by Rayleigh–Taylor instability. *Phys. Fluids A*, **3**, 5.

YOUNGS, D.L. (1992). A two-dimensional turbulence model based on the equations of multiphase flow. *The Third Zababakhin Scientific Talks*. Kyshtym, Dalnjaja dacha. Abstracts.